Journal of Zhejiang University SCIENCE A
ISSN 1673-565X (Print); ISSN 1862-1775 (Online)
www.zju.edu.cn/jzus; www.springerlink.com
E-mail: jzus@zju.edu.cn

Numerical simulation of a direct internal reforming solid oxide fuel cell using computational fluid dynamics method*

Jun LI†[1], Ying-wei KANG[1], Guang-yi CAO[1], Xin-jian ZHU[1], Heng-yong TU[1], Jian LI[2]

([1]*Institute of Fuel Cell, Department of Automation, Shanghai Jiao Tong University, Shanghai 200240, China*)

([2]*College of Materials Science and Engineering, Huazhong University of Science and Technology, Wuhan 430074, China*)

†E-mail: jun.li.fc@gmail.com

Received Nov. 12, 2007; revision accepted Feb. 27, 2008

Abstract: A detailed mathematical model of a direct internal reforming solid oxide fuel cell (DIR-SOFC) incorporating with simulation of chemical and physical processes in the fuel cell is presented. The model is developed based on the reforming and electrochemical reaction mechanisms, mass and energy conservation, and heat transfer. A computational fluid dynamics (CFD) method is used for solving the complicated multiple partial differential equations (PDEs) to obtain the numerical approximations. The resulting distributions of chemical species concentrations, temperature and current density in a cross-flow DIR-SOFC are given and analyzed in detail. Further, the influence between distributions of chemical species concentrations, temperature and current density during the simulation is illustrated and discussed. The heat and mass transfer, and the kinetics of reforming and electrochemical reactions have significant effects on the parameter distributions within the cell. The results show the particular characteristics of the DIR-SOFC among fuel cells, and can aid in stack design and control.

Key words: Direct internal reforming (DIR), Solid oxide fuel cell (SOFC), Computational fluid dynamics (CFD), Numerical simulation

doi:10.1631/jzus.A0720054 **Document code:** A **CLC number:** TM911.4

INTRODUCTION

With the rapid development of human society, environment and energy problems become the focus of study. Many scholars and engineers devote themselves to the energy field to develop an excellent device for future power plants that can produce clean electrical energy at high conversion rates. The solid oxide fuel cell (SOFC) is a kind of high temperature fuel cell (600 °C~1000 °C) that operates via a completely solid-state ion-conducting electrolyte (Larminie and Dicks, 2000; Zitouni *et al.*, 2007). The SOFC converts the chemical energy of a fuel directly into electrical energy. The electrical efficiency of an SOFC can reach 55% (Larminie and Dicks, 2000). Further, with the aid of catalyst, the SOFC can be directly fueled with natural gas and other hydrocarbons. Compared with indirect internal reforming SOFC (IIR-SOFC) and hydrogen-fueled SOFC stacks (Achenbach, 1994; Chan *et al.*, 2002), a direct internal reforming solid oxide fuel cell (DIR-SOFC) stack has different reaction kinetics. The electrochemical reactions interact with concurrent reforming reactions. It raises difficulties in analysis and design of the DIR-SOFC stack.

It is well known that the distributions of the parameters in the fuel cells are important for the designing and controlling of fuel cells. However, the information of the distribution, particularly for the DIR-SOFC at high operating temperature, is hardly to be obtained by measuring methods due to the limitations of sensors and high cost of experiments. It is the reason that an alternative way, fuel cells modeling becomes attractive. A 3D steady-state model was presented by Hu *et al*.(2004) to study the electro-

* Project (No. 2006AA05Z148) supported by the Hi-Tech Research and Development Program (863) of China

chemical and fluid behaviors in proton exchange membrane fuel cells (PEMFCs) with two kinds of flow fields (conventional and interdigitated). Achenbach (1994) modeled the temperature dynamics of an SOFC in a 3D vector space, which concentrated on the effects of temperature changes on output voltage response. A model of a molten carbonate fuel cell (MCFC) stack was developed by He and Chen (1998) and the simulation was implemented using a computational technique to investigate the 3D parameter distributions. Chan *et al.*(2002) presented two models to conduct the analysis of the energy and exergy in an SOFC system, and further proposed different level models (Chan *et al.*, 2003) to study the performance of the SOFC coupling with gas turbines. Aguiar *et al.*(2002; 2004) developed models for IIR-SOFC and DIR-SOFC respectively to simulate the 1D parameter distributions. A 1D dynamic model of a tubular SOFC with external and internal reforming was proposed by Jiang *et al.*(2006) to investigate characteristics under different work conditions.

In this paper, a 2D dynamic model of the DIR-SOFC is constructed based on the methane steam-reforming kinetics, electrical behavior, mass conservation and energy balance. The computational fluid dynamics (CFD) technique is applied to solving the complicated multiple partial differential equations (Bose, 1988; Al-Baghdadi and Al-Janabi, 2007). The numerical dynamic model of DIR-SOFC is developed in MATLAB. A cross-flow fuel cell is selected as an example to study the parameter distributions (temperature, species concentration and current density).

PRINCIPLES OF A DIR-SOFC

Fig.1 illustrates a cross-flow stack mainly constructed of gas manifolds, base plate, stack walls and a series of repeated cells. Each cell contains a layer of fuel gas, a layer of oxidant gas and a layer of anode-electrolyte-cathode (AEC) sandwiched by two half-separators. The fuel and air flow in two mutually-perpendicular directions, respectively. A schematic diagram of a DIR-SOFC is shown in Fig.2. At the anode, the methane-steam gas is reformed inside to generate H_2 and CO for the electrochemical reactions. At the cathode, combining with electrons, O_2 decomposes into O^{2-} due to the function of the catalyst. O^{2-} passes through the electrolyte and reacts with H_2 and CO to form H_2O and CO_2, respectively. The released electrons are output to drive the external load, and return to the cathode finally (Larminie and Dicks, 2000). The reforming and electrochemical reactions are given as follows.

Reforming reactions:

$$CH_4+2H_2O \leftrightarrow CO_2+4H_2, \quad (1)$$

$$CH_4+H_2O \leftrightarrow CO+3H_2, \quad (2)$$

$$CO+H_2O \leftrightarrow CO_2+H_2. \quad (3)$$

Electrochemical reactions:

anode:

$$H_2+O^{2-} \rightarrow H_2O+2e^-, \quad (4)$$

$$CO+O^{2-} \rightarrow CO_2+2e^-; \quad (5)$$

cathode:

$$\frac{1}{2}O_2+2e^- \rightarrow O^{2-}. \quad (6)$$

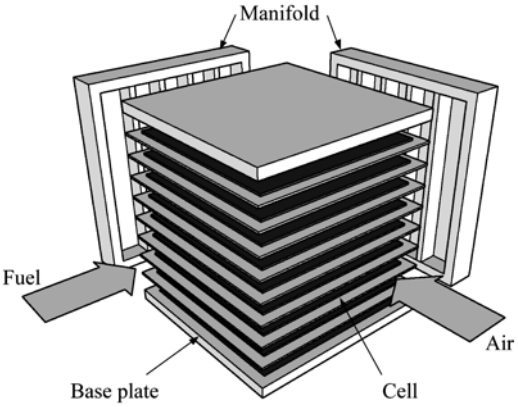

Fig.1 Scheme of a cross-flow stack

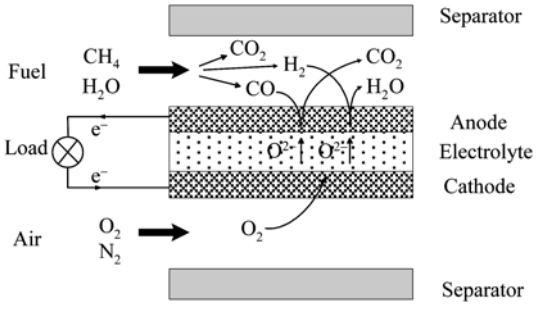

Fig.2 Schematic diagram of a DIR-SOFC

The separators clamp together the electrodes and electrolyte, and reinforce the cell units. Further, the separators with machined channels determine the kind of the flow field of fuel cells, and act as polar plates to collect the electrical current.

MATHEMATICAL MODEL

The mathematical model of the DIR-SOFC includes four main parts (reforming reactions, electrical power generation, mass conservation and energy balance) to describe the different behaviors occurring in the stack. The following main assumptions are made to develop the DIR-SOFC model: (1) The walls of the gas channels are smooth; (2) Gas flows in the stack are laminar; (3) All gases are ideal gases; (4) No gas phase reactions occur; (5) The electrolyte, anode and cathode layers are horizontally homogenous; (6) Methane does not directly participate in the electrochemical reaction at the anode; (7) The mass transfer resistance through the porous anode is ignored because of its small thickness and comparatively high H_2 diffusivity; (8) The modes of heat transfer contain conduction, convection and radiation. Heat transfer by radiation occurs only between the solid materials. The radiant heat between the fluid and the solid is negligible because it is very small relative to other heat transfers (conduction and convection between the fluid and the solid).

Reforming reactions

A $La_{0.75}Sr_{0.25}Cr_{0.5}Mn_{0.5}O_3/Gd_{0.2}Ce_{0.8}O_{1.9}$ (LSCM/GDC) composite electrode was developed by Chen *et al.*(2007a; 2007b). Further, they applied the LSCM/GDC as an SOFC anode to function with different fuel mixtures (weakly humidified hydrogen and methane (Chen *et al*., 2007a) and sulfur-containing methane (Chen *et al*., 2007b)). The experimental results showed high performance of the LSCM/GDC anode which had better hydrocarbon stability and sulfur tolerance under SOFC operating condition. Xu and Froment (1989) studied the methane steam reforming, methanation and water-gas shift based on a $Ni/MgAl_2O_4$ catalyst, and detailedly presented formulae to describe their intrinsic kinetics. For the purpose of this study, the Nickel catalyzed rate data proposed in (Xu and Froment, 1989) are used. Nickel is also assumed to be active for the oxidation at the anode.

Reactions Eqs.(1) and (2) are the dominant endothermic reactions in the reforming process. Reaction Eq.(3) is the water-gas shift reaction. The rates of the three reactions are respectively calculated by

$$r_1=\frac{k_1}{P_{H_2}^{3.5}D^2}\left(P_{CH_4}P_{H_2O}^2-\frac{P_{H_2}^4P_{CO_2}}{K_1}\right), \tag{7}$$

$$r_2=\frac{k_2}{P_{H_2}^{2.5}D^2}\left(P_{CH_4}P_{H_2O}-\frac{P_{H_2}^3P_{CO}}{K_2}\right), \tag{8}$$

$$r_3=\frac{k_3}{P_{H_2}D^2}\left(P_{CO}P_{H_2O}-\frac{P_{H_2}P_{CO_2}}{K_3}\right), \tag{9}$$

where K_1, K_2 and K_3 are the chemical equilibrium constants for reactions Eqs.(1)~(3), respectively, and P is the partial pressure (bar, 1 bar=10^5 Pa). k_1, k_2, k_3 and D are the rate coefficients and denominator that are dependent on operating conditions, respectively (Xu and Froment, 1989). The equilibrium constants are given by

$$K_1=\exp\left(-\frac{22430}{T}+26.078\right), \tag{10}$$

$$K_2=\exp\left(-\frac{26830}{T}+30.114\right), \tag{11}$$

$$K_3=\exp\left(\frac{4400}{T}-4.036\right), \tag{12}$$

where T is the operating temperature (K).

Electrical power generation

The cell voltage depends on reactants' partial pressures, stack configuration and operating temperature. Because data in (Vernoux *et al*., 1998; Georges *et al*., 2006) show that the electrochemical oxidation of H_2 is faster than that of CO, in this study, it is assumed that the electrochemical conversion rate of CO is negligible compared to that of H_2. The Nernst voltage, E, is mainly determined by the electrochemical reaction of H_2:

$$E=E_0+\frac{RT}{2F}\ln\left(\frac{P_{H_2}^{an}\sqrt{P_{O_2}^{ca}}}{P_{H_2O}^{an}}\right), \tag{13}$$

where E_0 is the EMF (electro-motive-force) (V) at standard pressure; R is the gas constant (8.314 J/(mol·K)); F is the Faraday constant (96485 C/mol); superscripts "an" and "ca" denote the anode and cathode, respectively.

The output voltage V_{out} will be lower than E, due to the ohmic loss η^{ohm}, activation overvoltage η^{act} and concentration loss η^{conc} (Achenbach, 1994; Aguiar *et al*., 2002; 2004):

$$V_{out} = E - \eta^{ohm} - \eta^{act} - \eta^{conc}, \tag{14}$$

where η^{ohm}, η^{act} and η^{conc} are the functions of temperature, current density and operating pressure, respectively. The relation between the output voltage and the current density can be expressed by

$$V_{out} = E + \eta^{loss}(i, P, T), \tag{15}$$

where i is the current density (A/m^2). The function η^{loss} is obtained by identification based on artificial neural networks.

The consumption rates of H_2 and O_2 in the electrochemical reactions (r_{H_2}, r_{O_2}) are directly related to the current density that can be obtained from Eq.(15):

$$r_{H_2} = i/(2F), \tag{16}$$

$$r_{O_2} = i/(4F). \tag{17}$$

Mass conservation

Because of the comparatively high diffusivity and small thickness of the gas flow layer, the time required to distribute the generated gases in the local area is ignored, and the gas in each element (divided by a computational grid) is assumed to be well-mixed.

The conservation equation of chemical species is given as

$$\frac{\mathrm{d}\boldsymbol{m}}{\mathrm{d}t} = \boldsymbol{M}_{in} - \boldsymbol{M}_{out} + \boldsymbol{B}\begin{bmatrix} -1 & -1 & 0 & 0 \\ 1 & 0 & 1 & 0 \\ 0 & 1 & -1 & 0 \\ 4 & 3 & 1 & -1 \\ -2 & -1 & -1 & 1 \\ 0 & 0 & 0 & -\frac{1}{2} \end{bmatrix}\boldsymbol{r}, \tag{18}$$

where $\boldsymbol{m}$ is the mass vector; $\boldsymbol{M}$ is the flow rate vector; subscripts "in" and "out" respectively denote the inlet and the outlet; $\boldsymbol{B}$ is a matrix in which elements are functions of the reaction area and molar mass; $\boldsymbol{r}$ is the reaction rate vector. $\boldsymbol{m}$, $\boldsymbol{M}$, $\boldsymbol{r}$ and $\boldsymbol{B}$ are respectively given as

$$\boldsymbol{m} = (m_{CH_4}, m_{CO_2}, m_{CO}, m_{H_2}, m_{H_2O}, m_{O_2})^{\mathrm{T}}, \tag{19}$$

$$\boldsymbol{M} = (M_{CH_4}, M_{CO_2}, M_{CO}, M_{H_2}, M_{H_2O}, M_{O_2})^{\mathrm{T}}, \tag{20}$$

$$\boldsymbol{r} = (r_1, r_2, r_3, r_{H_2})^{\mathrm{T}}, \tag{21}$$

$$\boldsymbol{B} = \mathrm{diag}\left(A^{an}W_{CH_4}, A^{an}W_{CO_2}, A^{an}W_{CO}, A^{an}W_{H_2}, A^{an}W_{H_2O}, A^{ca}W_{O_2}\right), \tag{22}$$

where A^{an} and A^{ca} are anodic and cathodic reaction areas (m^2), respectively, and W is the molar mass (kg/mol).

Energy balance

The methane steam-reforming reaction is endothermic and needs much steam. The electrochemical reaction is exothermic and produces a large amount of heat and steam for the reforming reaction. In fuel cells, the rate distributions of the reforming and electrochemical reactions are not uniform, because of the different operating conditions (species concentrations, temperature, etc.) across the cells. Hence, the temperatures are not even in the stack, which results in heat transfer among the components of the stack. The heat convection between the solid parts and the gas flows, the heat radiation between different solid parts and the heat conduction are taken into account, except the radiant heat transfer between the gas flow and the solid (assumption (8)). The outer walls of the fuel cell are assumed to be insulated, and have no heat exchange with the surrounding environment. Besides the electrical power output and heat transferred in the stack, the heat generated in the electrochemical reactions flows out of the stack with the exhaust gases.

For the air and fuel flows, the energy equation can be given as

$$\frac{\partial(\rho h)}{\partial t} + \mathrm{div}\left(\rho h\boldsymbol{V} - \frac{\zeta\nabla h}{C_p}\right) = S_h, \tag{23}$$

where ρ is the density (kg/m^3); h is the gas enthalpy

(J/kg); ζ is the thermal conductivity (W/(m·K)); C_p is the specific heat capacity (J/(kg·K)); $\boldsymbol{V}$ is the gas velocity vector (m/s); div denotes the divergence; ∇ denotes the gradient; and S_h is the heat source.

The energy equation for the solid part can be simplified as

$$\rho C_p \frac{\partial T}{\partial t} - \mathrm{div}(\zeta \nabla T) = S_h. \quad (24)$$

We assume that the reforming and electrochemical reactions (reactions Eqs.(1), (2), (4) and (6)) occur in the AEC, and the water-gas shift reaction (reaction Eq.(3)) mainly occurs in the fuel channel.

S_h for the air and separators is zero. For the AEC, the heat source S_h is generated by the reforming, electrochemical reactions and electrical current, i.e.,

$$S_h = \left(-\Delta H_1 r_1 - \Delta H_2 r_2 - \Delta H_e r_{H_2} - V_{out} i\right) \Big/ \delta^{AEC}, \quad (25)$$

where ΔH_e, ΔH_1 and ΔH_2 are enthalpy changes (J/mol) of the electrochemical reaction, reactions Eqs.(1) and (2), respectively; δ^{AEC} is the thickness of the AEC (m).

The heat source for the fuel is generated by the water-gas shift reaction, i.e.,

$$S_h = -\Delta H_3 r_3 \big/ \delta^{fuel}, \quad (26)$$

where ΔH_3 is the enthalpy change (J/mol) of the water-gas shift reaction; δ^{fuel} is the thickness of the fuel channel (m).

NUMERICAL APPROACH

From previous sections, we see that the problems in the fuel cell operation usually require solution of multiple partial differential equations (PDEs) with given boundary conditions. These problems can be treated in a rigorous manner only in the case of simple boundaries. Because of the complex operating conditions of the DIR-SOFC, a rigorous solution cannot be obtained, and a numerical approach can be the alternative choice. Computational fluid dynamics (CFD) is a kind of numerical method that has been applied to the analysis of systems involving fluid flow, heat transfer and associated phenomena such as chemical reactions (Bose, 1988; Ferziger and Peric, 1996).

The planar fuel cell is divided into elements to generate a computational grid. The operating mode of the SOFC studied in this paper is the cross-flow, hence, the fuel and air are assumed to flow in the x and y directions, respectively. In the z direction, there are five control volumes: upper separator, fuel, AEC, air and lower separator. The heat is transferred between them by means of convection and radiation. In the solid parts and gases, the heat conduction is also involved. At the fuel and air inlets, flow rates, chemical species concentrations, pressures and temperatures of gases are set as constants.

In the calculations, the CFD code is used for solving the finite-volume Navier-Stokes and transport equations to obtain the fuel and air flow rates, chemical species concentrations and temperature at each location in the cell. The reforming and electrochemical models are functions of partial pressures and temperature. Hence, using the numerical solutions obtained by the CFD code, we can calculate the local reforming reaction rates and voltage-current density curves. The local electrochemical reaction rates of H_2 and O_2 can thus be obtained. Then the information is used for calculating the heat source, species sources and new distributions of gas species concentrations, current density and temperature for the next iteration. These steps are repeated until conditions in the cell reach a steady state.

RESULTS AND DISCUSSION

The cell parameters and operating conditions are listed in Table 1. Combining the equations in previous sections, the numerical model of the DIR-SOFC is implemented in MATLAB using the CFD method. In the computational process, the conditions in the fuel cell will evolve until the results converge. The steady-state distributions of chemical species concentrations, temperature and current density can be obtained.

The concentration distributions of CH_4, CO_2, CO, H_2, H_2O and O_2 are shown in Figs.3a~3f, respectively. Near the fuel inlet, the electrochemical reaction rate is relatively low due to the low H_2 concentration, resulting in the low consumption rates of H_2 and O_2. In this study, the air is sufficient, and the utilizations of fuel and oxygen are 68% and 21%, respectively. Thus,

Table 1 Cell specifications and operating conditions

Parameter	Value	Parameter	Value
Cell size (m×m)	0.43×0.43	Electrolyte heat capacity (J/(kg·K))	606
Separator thickness (m)	2×10^{-3}	Cathode thickness (m)	1×10^{-4}
Separator thermal conductivity (W/(m·K))	25	Cathode thermal conductivity (W/(m·K))	2.16
Separator density (kg/m^3)	8000	Cathode density (kg/m^3)	3310
Separator heat capacity (J/(kg·K))	500	Cathode heat capacity (J/(kg·K))	573
Separator emissivity	0.1	Cathode emissivity	0.7
Anode thickness (m)	2×10^{-3}	Pressure (Pa)	3×10^{5}
Anode thermal conductivity (W/(m·K))	2	Out voltage (V)	0.65
Anode density (kg/m^3)	3030	Inlet fuel flow rate (kg/s)	2.7×10^{-5}
Anode heat capacity (J/(kg·K))	595	Inlet air flow rate (kg/s)	4×10^{-4}
Anode emissivity	0.7	Inlet fuel temperature (K)	1024
Electrolyte thickness (m)	4×10^{-5}	Inlet air temperature (K)	1024
Electrolyte thermal conductivity (W/(m·K))	2	Fuel composition CH_4:CO_2:CO:H_2:H_2O	29:1:1:9:60
Electrolyte density (kg/m^3)	5160	Air composition O_2:N_2	24:76

the change of the air flow rate along the air flow direction near the fuel inlet is very small. It causes the negligible change of air cooling effect along the same direction (However, the change of air cooling effect is large along the fuel flow direction, because of the increased consumption rate of O_2). Hence, the temperature gradients near the fuel inlet along the air flow direction are relatively small. Further, the calculation formulae of reaction rates are functions of temperature. As a result, the chemical species (including CH_4, CO_2, CO, H_2 and H_2O) concentration changes are not large in general along the same direction near the fuel inlet.

Due to the consumption of CH_4 in the reforming reactions, the CH_4 concentration gradually decreases along the fuel flow direction as can be seen in Fig.3a. The concentrations of CO_2 and CO gradually increase with the fuel flow as shown in Figs.3b and 3c. In Fig.3d, along the fuel flow direction, the H_2 concentration gradually increases at first, because of the methane reforming. When the fuel reaches the second half of the fuel channel, most of CH_4 has been reformed. H_2 produced in the methane reforming is not sufficient for compensating the consumption of H_2 in the electrochemical reaction. Therefore, the H_2 concentration begins to decrease after the initial increase. Because the methane reforming needs a large amount of steam, which, in excess of twice as much as the methane, is injected into the fuel cell with the fuel. As shown in Fig.3e, the H_2O concentration decreases at first caused by the rapid reforming reactions near the fuel inlet, and then increases due to the increase of the product H_2O in the intensified electrochemical reaction. In Fig.3f, the O_2 concentration gradually decreases along the air flow direction, and reaches its minimum value near the air outlet and the center of the fuel channel.

The temperature distribution on the AEC and the corresponding contours are shown in Figs.4a and 4b, respectively. The current density distribution and the corresponding contours are given in Figs.5a and 5b, respectively. As shown in Fig.4b, the local temperature near the fuel inlet falls down to a level that is lower than the inlet fuel temperature (1024 K). This is because a lot of heat is lost in the fast endothermic reforming reactions resulting from the large CH_4 concentration near the fuel inlet. At the same position, the H_2 concentration is relatively low, resulting in the slow electrochemical reaction and the small local current density (Fig.5b). The generated heat is thus not enough to make up for the heat losses in the reforming reactions.

With the increase of H_2 concentration as shown in Fig.3d, the local electrochemical reaction rate and the corresponding local current density (Fig.5b) increase. Thus, the generated heat in excess of the heat losses can raise the local temperature. The maximum local current density is located around the center of the fuel channel near the air outlet where the local temperature (Fig.4b) and the H_2 concentration (Fig.3d) are close to their maximum values. Therefore, the O_2 concentration (Fig.3f) reaches its minimum values

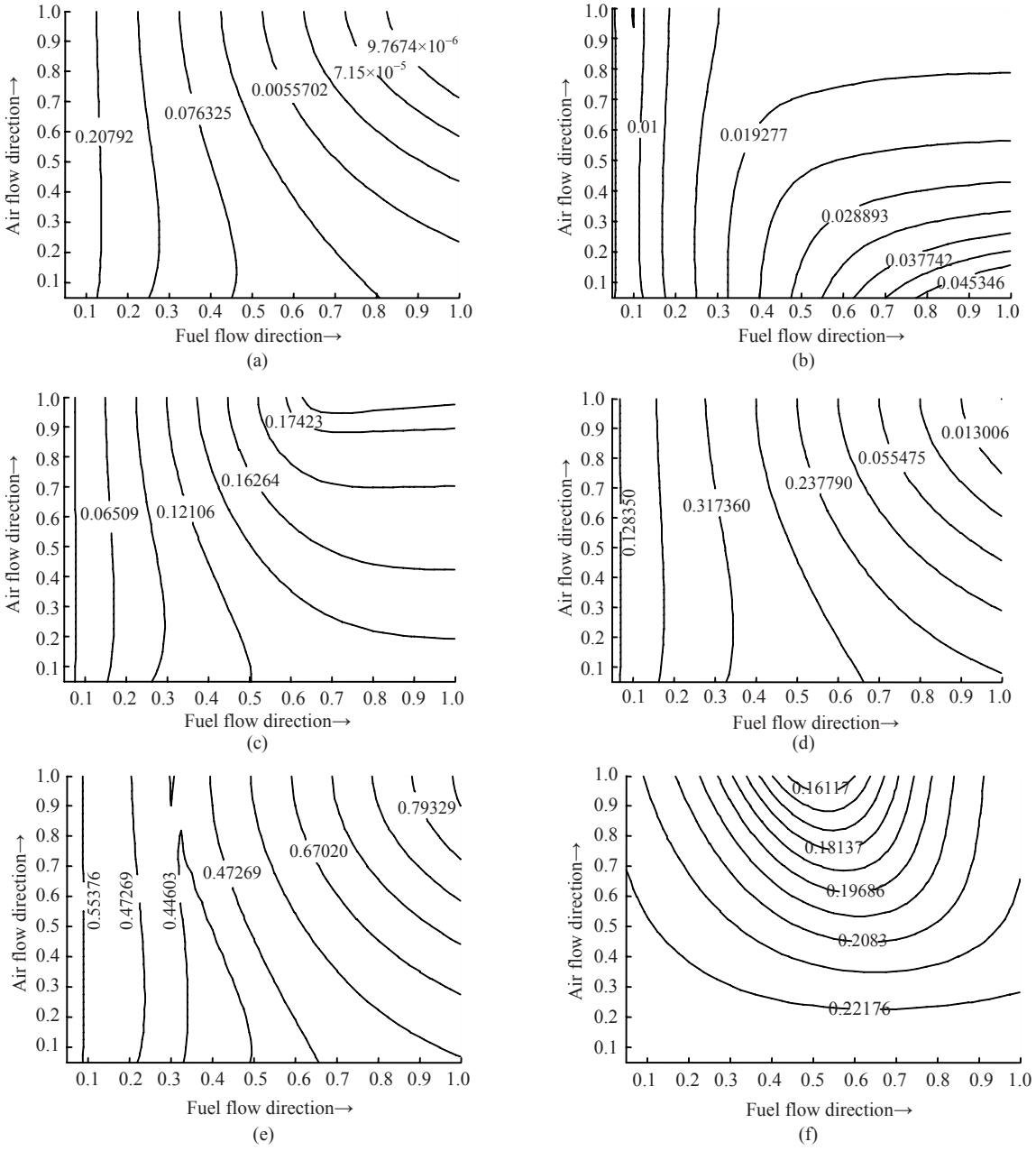

Fig.3 (a) CH_4, (b) CO_2, (c) CO, (d) H_2, (e) H_2O and (f) O_2 concentration distribution (mol/mol)

around the same position. In the second half of the fuel channel (Fig.5b), the trend in current density is decreasing in the direction of the fuel flow. Due to the convective heat transfer from the AEC to the air flow, the temperature rises gradually in the air flow direction (Figs.4a and 4b).

To reveal the temperature distribution in the *z* direction (perpendicular to the fuel and air flow directions), the temperature distributions of the AEC, fuel and air are plotted in Fig.6. Figs.7a and 7b show the temperature distributions of the AEC, fuel and air along the fuel flow direction at y=0.3 and y=0.975, respectively. In the low temperature area (near the fuel and air inlets) of Fig.6, e.g., 1003 K, the AEC temperature contour surrounds the contours of the fuel and air. It is indicated more clearly in Fig.7a that the AEC temperature is lower than the temperatures of the fuel and air in this area. In the high temperature region, e.g., 1250 K, the AEC temperature contour also surrounds the other two contours. Different from

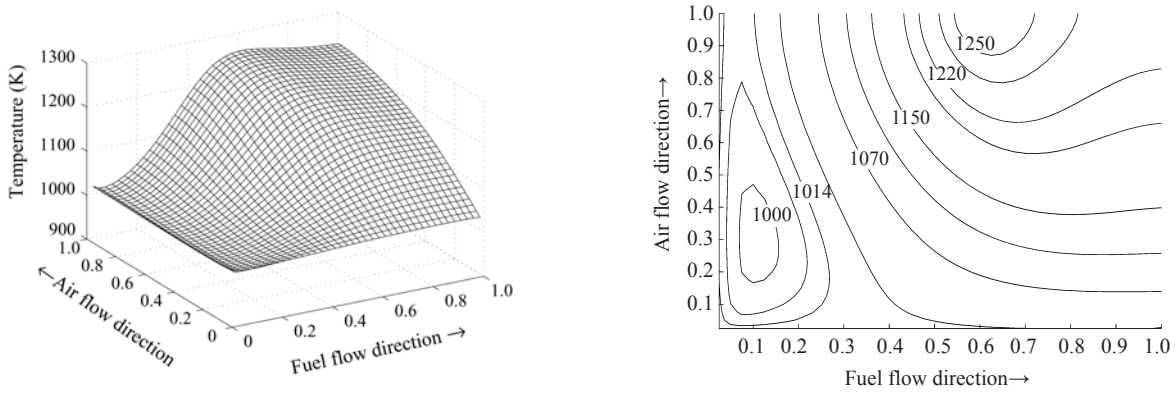

(a) (b)

Fig.4 Temperature distribution on the AEC (a) and the corresponding contours (b)

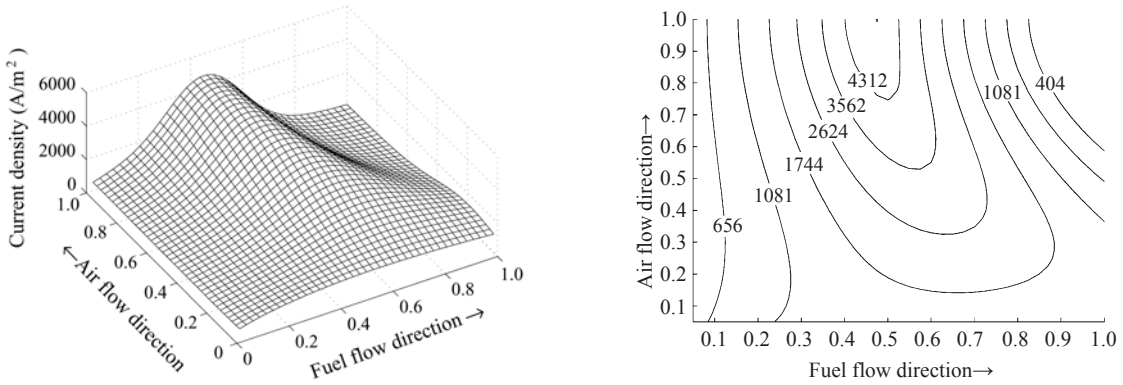

(a) (b)

Fig.5 Current density distribution on the AEC (a) and the corresponding contours (b)

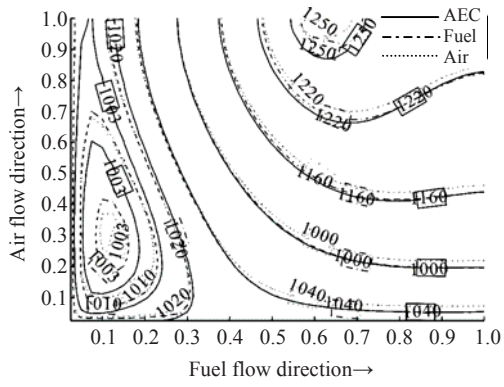

Fig.6 Comparison of temperature (K) distributions of AEC, fuel and air

the case of 1003 K, it can be seen from Fig.7b that the AEC temperature is higher than others. This is because we assume that the endothermic reforming and exothermic electrochemical reactions occur in the AEC (due to the function of the catalyst). As a result, the temperature changes of gases lag behind that of AEC.

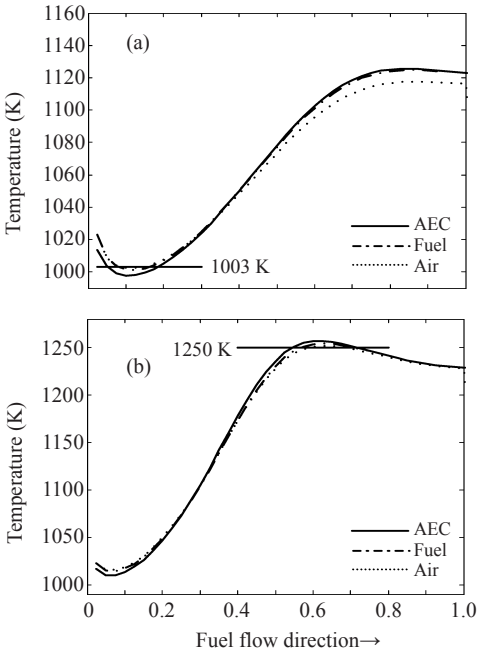

Fig.7 Temperature distribution along the fuel flow direction at (a) y=0.3 and (b) y=0.975

CONCLUSION

A mathematical model of a DIR-SOFC is built based on the methane steam-reforming kinetics, electrical behavior, mass conservation and energy balance. The numerical simulation is performed in MATLAB using CFD method. The steady-state distributions of chemical species concentrations, temperature and current density in the cross-flow DIR-SOFC are illustrated to investigate the performance of the DIR-SOFC. The results show that the parameters such as species concentrations, temperature and current density influence interactively. The steady-state parameter distributions and behavior of the DIR-SOFC are different from the SOFC fueled with pure hydrogen. The results can be used in designing and controlling of the DIR-SOFC.

References

Achenbach, E., 1994. 3D and time-dependent simulation of a planar solid oxide fuel cell stack. *Journal of Power Sources*, **49**(1-3):333-348. [doi:10.1016/0378-7753(93)01833-4]

Aguiar, P., Chadwick, D., Kershenbaum, L., 2002. Modelling of an indirect internal reforming solid oxide fuel cell. *Chemical Engineering Science*, **57**(10):1665-1677. [doi:10.1016/S0009-2509(02)00058-1]

Aguiar, P., Adjiman, C.S., Brandon, N.P., 2004. Anode-supported intermediate-temperature direct internal reforming solid oxide fuel cell. I: model-based steady-state performance. *Journal of Power Sources*, **138**(1-2):120-136. [doi:10.1016/j.jpowsour.2004.06.040]

Al-Baghdadi, M.A.R.S., Al-Janabi, H.A.K.S., 2007. Optimization study of a PEM fuel cell performance using 3D multi-phase computational fluid dynamics model. *Journal of Zhejiang University SCIENCE A*, **8**(2):285-300. [doi:10.1631/jzus.2007.A0285]

Bose, T.K., 1988. Computational Fluid Dynamics. Wiley Eastern Limited, New Delhi, p.6.

Chan, S.H., Low, C.F., Ding, O.L., 2002. Energy and exergy analysis of a simple solid-oxide fuel cell power system. *Journal of Power Sources*, **103**(2):188-200. [doi:10.1016/S0378-7753(01)00842-4]

Chan, S.H., Ho, H.K., Tian, Y., 2003. Multi-level modeling of SOFC-gas turbine hybrid system. *International Journal Hydrogen Energy*, **28**(8):889-900. [doi:10.1016/S0360-3199(02)00160-X]

Chen, X.J., Liu, Q.L., Chan, S.H., Brandon, N.P., Khor, K.A., 2007a. High performance cathode-supported SOFC with perovskite anode operating in weakly humidified hydrogen and methane. *Electrochemistry Communications*, **9**(4):767-772. [doi:10.1016/j.elecom.2006.11.012]

Chen, X.J., Liu, Q.L., Chan, S.H., Brandon, N.P., Khor, K.A., 2007b. Sulfur tolerance and hydrocarbon stability of $La_{0.75}Sr_{0.25}Cr_{0.5}Mn_{0.5}O_3/Gd_{0.2}Ce_{0.8}O_{1.9}$ composite anode under anodic polarization. *Journal of the Electrochemical Society*, **154**(11):B1206-B1210. [doi:10.1149/1.2780866]

Ferziger, J.H., Peric, M., 1996. Computational Methods for Fluid Dynamics. Springer-Verlag, New York, p.10.

Georges, S., Parrour, G., Henault, M., Fouletier, J., 2006. Gradual internal reforming of methane: a demonstration. *Solid State Ionics*, **177**(19-25):2109-2112. [doi:10.1016/j.ssi.2006.01.033]

He, W., Chen, Q., 1998. 3D simulation of a molten carbonate fuel cell stack under transient conditions. *Journal of Power Sources*, **73**(2):182-192. [doi:10.1016/S0378-7753(97)02800-0]

Hu, G.L., Fan, J.R., Chen, S., Liu, Y.J., Cen, K.F., 2004. 3D numerical analysis of proton exchange membrane fuel cells (PEMFCs) with conventional and interdigitated flow fields. *Journal of Power Sources*, **136**(1):1-9. [doi:10.1016/j.jpowsour.2004.05.010]

Jiang, W., Fang, R.X., Khan, J.A., Dougal, R.A., 2006. Parameter setting and analysis of a dynamic tubular SOFC model. *Journal of Power Sources*, **162**(1):316-326. [doi:10.1016/j.jpowsour.2006.06.086]

Larminie, J., Dicks, A., 2000. Fuel Cell Systems Explained. Wiley, New York, p.164.

Vernoux, P., Guindet, J., Kleitz, M., 1998. Gradual internal methane reforming in intermediate-temperature solid-oxide fuel cells. *Journal of the Electrochemical Society*, **145**(10):3487-3492. [doi:10.1149/1.1838832]

Xu, J.G., Froment, G.F., 1989. Methane steam reforming, methanation and water-gas shift: I. intrinsic kinetics. *AIChE Journal*, **35**(1):88-96. [doi:10.1002/aic.690350109]

Zitouni, B., Ben, Moussa, H., Oulmi, K., 2007. Studying on the increasing temperature in IT-SOFC: Effect of heat sources. *Journal of Zhejiang University SCIENCE A*, **8**(9):1500-1504. [doi:10.1631/jzus.2007.A1500]